Assessment of Energy-Weighted Acquisition in SPECT Using ROC Analysis

Roger T. Staff, Howard G. Gemmell and Peter F. Sharp

Department of Bio-Medical Physics and Bio-Engineering, University of Aberdeen, Aberdeen, Scotland

Energy-weighted acquisition is a technique for reducing Compton scatter effects in nuclear medicine images. The effect of energy-weighted acquisition on SPECT ^{99m}Tc images was evaluated by comparing the energy-weighted acquisition images with those obtained using a 20% photopeak energy window. **Methods:** SPECT images were compared using receiver operator characteristic (ROC) experiments testing the observer's ability to perform a pseudoclinical task. The tasks were detecting cold lesions within a uniform background and cold lesions within images created with a tomographic brain phantom. **Results:** ROC analysis for each phantom produced different results. No significant difference was found between the two acquisition techniques in detecting cold lesions on uniform backgrounds. Energy-weighted acquisition improved cold lesion detection significantly within the brain phantom in comparison with 20% photopeak acquisition. **Conclusion:** Lesion detection in ^{99m}Tc SPECT images can be improved using energy-weighted acquisition. This improvement, however, is dependent on the nature of the object being imaged. Images with structure show improved detection, whereas uniform images do not.

Key Words: scatter correction; single-photon emission computed tomography; receiver operating characteristics analysis; cold lesions

J Nucl Med 1995; 36:2352–2355

The conventional method of rejecting scattered photons detected by a gamma camera is to use a discrete energy window centered on the photopeak of primary unscattered radiation. Scatter rejection is, however, incomplete with this approach due to the imperfect energy resolution of scintillation detectors. Energy-weighted acquisition uses information from all detected scintillation events to reduce scatter effects. This approach has been implemented in the weighted-acquisition module manufactured by Siemens, Des Plaines, IL. The theory behind energy-weighted acquisition and weighted-acquisition module has been discussed previously by Hamill and DeVito (*1*) and DeVito et al. (*2*).

De Vito et al. and Halama et al. (*2,3*) investigated the effects of energy-weighted acquisition using a weighted-acquisition module on static and tomographic images and showed that weighted acquisition improves image contrast, which is highest with radionuclides that have multiple photopeaks such as ^{67}Ga and ^{201}Tl. Floyd et al. (*4*) investigated the effects of energy-weighted acquisition on ^{201}Tl myocardial SPECT images and concluded that energy-weighted acquisition yields ^{201}Tl images that are often more visually pleasing and have greater contrast than discrete energy windowing. Most clinical SPECT imaging is performed using ^{99m}Tc-based pharmaceuticals and SPECT imaging using agents such as hexamethylpropylineamine oxime (HMPAO) have a wide range of clinical applications (*5*). For this reason, we decided to conduct this investigation using ^{99m}Tc. Rao et al. (*6*) studied the effect of energy-weighted acquisition on clinical static ^{99m}Tc bone images and found no significant difference between 20% symmetrical photopeak imaging and energy-weighted acquisition using weighted-acquisition module. The experimental approach used in this work, however, was to simply count the number of lesions seen in the bone images of 97 patients. This technique is far from ideal because it only assesses the relative sensitivities of the two acquisition procedures and pays no attention to their specificities.

According to Halama et al. (*3*), energy-weighted acquisition can generate "images of greater diagnostic quality than can be achieved with conventional energy windowing methods." The concept of diagnostic quality, however, has not been clearly defined. Sharp (*7*) suggested that quality is a task-dependent phenomenon. Therefore, we decided to compare energy-weighted acquisition and discrete energy window as a pseudoclinical task using two ROC (receiver operator characteristics) experiments to test the observer's ability to detect a cold lesion positioned within a reconstructed tomographic image. Each ROC experiment was performed using a different tomographic phantom.

METHODS

Phantoms

The ROC experiments were carried out using two different tomographic phantoms: one with a structureless background while the other was a brain phantom. The first consisted of a hollow cylinder (220-mm diameter, 180-mm length) which had a removable Perspex rod positioned parallel to its long axis. The rod had a diameter of 16 mm and produced a cold lesion in the reconstructed image. The second phantom was the Hoffman brain phantom (*8*). A removable plasticine ball, approximately 16 mm in

Received Jul. 6, 1994; revision accepted Nov. 7, 1994.

For correspondence or reprints contact: Roger T. Staff, PhD, University of Aberdeen, Department of Bio-Medical Physics and Bio-Engineering, Foresterhill Aberdeen, AB9 2ZD, Scotland.

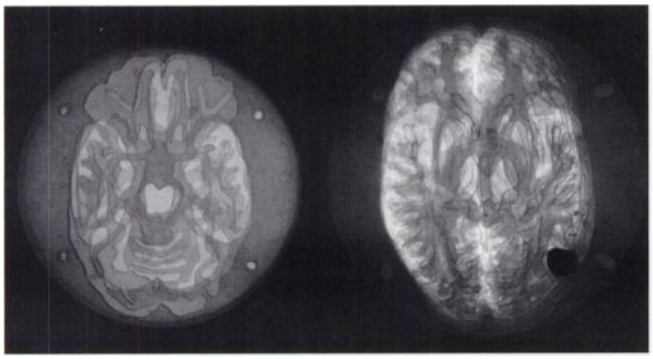

FIGURE 1. The Hoffman brain phantom with the plasticine ball. (Right) Phantoms slices (75%) viewed from below. (Left) Remaining phantoms slices (25%) viewed from above.

diameter (Fig. 1), was placed inside the phantom to create the cold lesion in the reconstructed image.

Data Acquisition

The phantoms were filled with approximately 400 MBq ^{99m}Tc and imaged on a Siemens Orbiter 7500 ZLC rotating gamma camera fitted with a general-purpose collimator. The phantoms were imaged using a 360° orbit to acquire 64 equally spaced projections collected into 64 × 64 word image arrays. The number of counts in the first projection image was 70 kcts, giving a count density similar to that found in clinical brain studies. All other projection frames were acquired for the same period of time as the first frame. The cylindrical phantom was imaged eight times: four times with the rod present and four times without the rod. The position of the rod within the phantom was varied each time the phantom was imaged in order to change the position of the cold lesion within the reconstructed image. This procedure was repeated twice: first with the weighted-acquisition module and then with discrete energy window acquisition. The Hoffman phantom was imaged a total of 32 times: 16 times with the plasticine ball present and 16 times without. When the phantom was imaged with the ball present, the ball's position was changed. This acquisition procedure was carried out twice: first using weighted-acquisition module and then using discrete energy window acquisition. The discrete energy window used a 20% window positioned symmetrically about the photopeak.

Image Reconstruction and Correction

Images were reconstructed on a Siemens Maxdelta data processing system using a filtered backprojection method. A generalized Hamming filter with a Nyquist frequency cutoff (0.83 cm^{-1}) and an alpha value of 0.5 was used. The data were corrected for center of rotation variations but were not flood-corrected because the flood correction procedure appeared to make the data worse. This occurrence has previously been noted by Elliot (*9*) who suggested that uniformity correction was not useful if the coefficient of variation of the flood image was less than 2–3%.

A first-order Chang correction technique (*10*) was used to correct the images for attenuation caused by the phantom. The linear attenuation coefficient was 0.15 cm^{-1}. A technique devised by Staff and Gemmell (*11*) was used to correct the considerable attenuation caused by the couch supporting the phantom.

Cylindrical phantom projection data were used to reconstruct and correct the 16 central slices from each projection dataset for a total of 256 images. This dataset had equal numbers of images produced with energy-weighted acquisition and discrete energy window and with and without the rod being present in the phantom. Eight central slices containing images of the plasticine ball were reconstructed from each Hoffman phantom projection dataset. A total of 32 sets of 8 images were reconstructed.

ROC Experiments

The images produced using the cylindrical phantom were randomly mixed and presented to four observers. The images were randomly rotated by 0°, 90°, 180° or 270° to further vary lesion position within the image. The observers were asked to state how confident they were that a cold lesion was present within the image on a scale of 1 to 6 (6 representing the most confident response and 1 representing the least confident response). The images were presented individually to the observers on a TV screen using the Siemens rainbow color scale. The observers were told that there was a maximum of one lesion present in each image but were not told the proportion of images without a cold lesion. The observers viewed all the images at one sitting.

A similar ROC experiment was performed with the Hoffman phantom images. This time, however, a set of eight images produced from each projection dataset were both presented on the screen. The observers viewed these image sets randomly and were asked to state how confident (again on a scale of 1 to 6) they were that a cold lesion was present somewhere within the eight images. As before, the observers were told there was a maximum of one lesion present in each image but not the proportion of images without a cold lesion. All the images were viewed at one sitting. Images similar to those used to conduct this experiment can be seen in Figure 2.

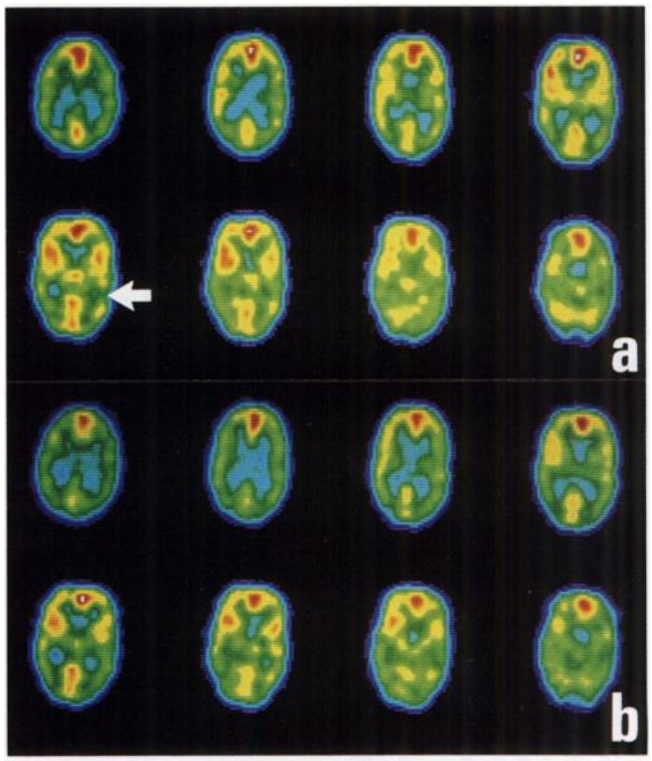

FIGURE 2. (a) Reconstructed images of the Hoffman brain phantom with the defect present created using energy-weighted acquisition. Lesion location is indicated by the arrow. (b) Reconstructed images of the Hoffman brain phantom with no defect present created using energy-weighted acquisition.

RESULTS

When a set of images is assessed by more than one observer under identical conditions, two approaches can be used to estimate a single ROC curve that describes the performance of all the observers. The individual datasets can be summed together, or pooled, to produce a single dataset which can have a ROC curve fitted, or each observer's data can have a curve fitted, the resultant ROC parameter estimated and then averaged over all observers to give an average ROC curve. Swets and Pickett (*12*) advocate the first method when observers have similar skills and suggest that the second technique may be preferable when a heterogeneous observer population is used.

Due to the relatively small number of images, pooling the individual responses to create an average observer dataset would be preferable. Since we did not know if the observer skills were similar, a correlated chi square comparison was done as described by Metz et al. (*13*).

Chi square comparisons between each observer are detailed in Tables 1 and 2. Chi square calculation was performed using the computer program CORROC (*14*). The chi square value above which a null hypothesis no longer holds is 5.6 for 2 degrees of freedom and a probability of 95%. The results show that there is no significant difference between the observers for data produced using each acquisition technique and that pooling the data to produce an average observer is valid. Figures 3 and 4 show the ROC curves for each acquisition technique for an average observer. The ROC curves were fitted to the measured points using a computer program known as ROCFIT (*15*). This program, based on an approach described by Dorfman et al. (*15*), creates a maximum likelihood estimate curve fit to the data points.

The area under a curve is a common figure of merit when assessing ROC curves (*14*). The area under the ROC curves for the average observer for each phantom are shown in Table 3 as well as correlated chi square comparisons between each acquisition technique for each phantom. For the cylindrical phantom, the area under the ROC curve is larger for the discrete energy window than for energy-weighted acquisition, but this difference is not statistically significant. The results for the Hoffman brain phantom show significantly improved observer performance when energy-weighted acquisition is used.

TABLE 1
Chi Square Comparison between Each Observer Using Images Created with a Cylindrical Phantom

Observer no.	2		3		4	
	EWA	DEW	EWA	DEW	EWA	DEW
1	0.94	0.69	2.21	2.67	2.71	0.48
2	—		2.18	3.81	4.20	1.13
3			—		0.18	2.54

EWA = energy-weighted acquisition and DEW = discrete energy window.

TABLE 2
Chi Square Comparison between Each Observer Using Images Created with the Hoffman Phantom

Observer no.	2		3		4	
	EWA	DEW	EWA	DEW	EWA	DEW
1	0.95	2.17	0.66	2.66	0.30	0.97
2	—		0.25	0.07	0.17	0.53
3			—		0.12	2.24

EWA = energy-weighted acquisition and DEW = discrete energy window.

DISCUSSION

The primary objective of this study was to compare energy-weighted acquisition and discrete energy window in detecting cold lesions. Floyd et al. (*4*) reported improvements in tomographic contrast and diagnostic performance when energy-weighted acquisition is used with multiple photopeak radionuclides such as ^{201}Tl. DeVito et al. (*2*) compared energy-weighted acquisition with discrete energy window using ^{99m}Tc in SPECT and found that energy-weighted acquisition improves contrast. Our results suggest that improved contrast does not necessarily imply an improvement in observer performance. The two ROC experiments in this work have conflicting results. There is no difference between energy-weighted acquisition and discrete energy window in detecting cold lesions on a uniform background produced with the cylindrical phantom, but energy-weighted acquisition significantly improves the ability of observers to detect a cold lesion within the recon-

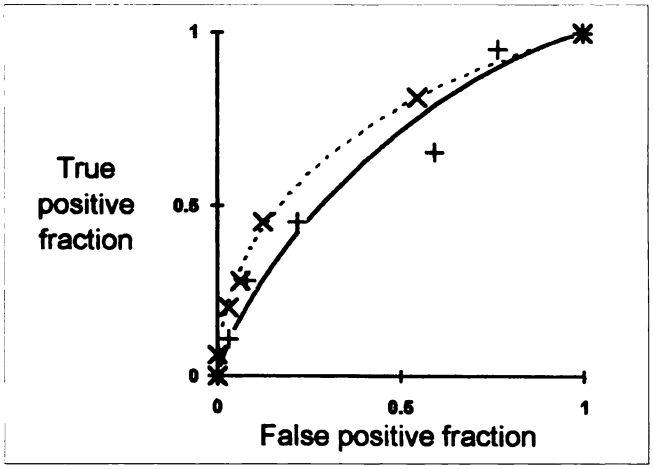

FIGURE 3. Energy-weighted acquisition and discrete energy window comparison of average observer ROC curves for the cold lesion on a hot uniform background detection task. Fitted energy-weighted acquisition (—); fitted discrete energy window (– – –); measured energy-weighted acquisition (+); measured discrete energy window (×).

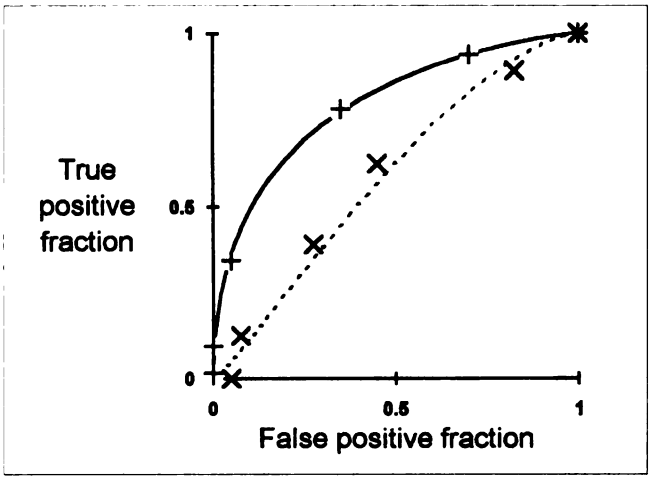

FIGURE 4. Comparison between energy-weighted acquisition and discrete energy window of average observer ROC curves for the cold lesion detection task using the Hoffman brain phantom. Fitted energy-weighted acquisition (—); fitted discrete energy window (– – –); measured energy-weighted acquisition (+); measured discrete energy window (×).

structed images of the Hoffman brain phantom. This difference may be due to the fact that energy-weighted acquisition produces count fluctuations that are spatially correlated (*3*). Although the effect of different spatial frequencies on image perception and observer performance is not clearly understood, observer performance is dependent on the signal and noise spatial frequency distribution (*17*). The spatial correlation or texture produced using energy-weighted acquisition is more apparent when the image has large uniform areas, such as those produced by the cylindrical phantom, than when the image has underlying structure, such as that produced by the Hoffman phantom. The ease with which the texture is seen may be responsible for the drop in performance in cold lesion detection within the cylindrical phantom. The task produced by the Hoffman phantom is closer to the clinical task in which underlying anatomical structure is present. Further study is required with actual clinical SPECT data to discover if this apparent change in observer performance translates into a real diagnostic improvement.

TABLE 3
Area under the ROC Curves for Each Phantom Using Average Observer Data

Phantom	Area under the DEW ROC curve	Area under the EWA photopeak ROC curve	χ^2
Cylindrical	0.73 (0.05)	0.65 (0.05)	2.03
Hoffman	0.58 (0.06)	0.79 (0.05)	9.08

The last column contains the values of chi square between the ROC curves produced using EWA and DEW. The values in parentheses represent the s.d. of the curve fit.

DEW = discrete energy window; EWA = energy-weighted acquisition; χ^2 = chi square.

REFERENCES

1. Hamill JJ, Devito RP. Scatter reduction with energy-weighted acquisition. *IEEE Trans Nucl Sci* 1989;36:1334–1339.
2. Devito RP, Hamill JJ, Treffert JD, Stoub EW. Energy-weighted acquisition of scintigraphic images using finite spatial filters. *J Nucl Med* 1989;30:2029–2035.
3. Halama JR, Henkin RE, Friend LE. Gamma camera radionuclide images: improved contrast with energy-weighted acquisition. *Radiology* 1988;169: 533–538.
4. Floyd JL, Mann RB, Shaw A. Changes in quantitative SPECT thallium-201 results associated with the use of energy-weighted acquisition. *J Nucl Med* 1990;32:805–807.
5. Holman BL, Devous MD. Functional brain SPECT: the emergence of a powerful clinical method. *J Nucl Med* 1992;33:1888–1904.
6. Rao MG. Bone imaging with energy-weighted acquisition. *J Nucl Med* 1993; 34:997–999.
7. Sharp PF. Quantifying image quality. *Clin Phys Physiol Meas* 1990;11(Suppl): 21–26.
8. Hoffman EJ, Cutler PD, Digby WM, Mezziontta JC. A three-dimensional phantom to simulate cerebral blood flow and metabolic images for PET. *IEEE Trans Nucl Sci* 1990;37:616–620.
9. Elliot AT. Quality control. In: Sharp PF, Gemmell HG, Smith FW, eds. *Practical nuclear medicine*. Oxford: IRL Press at Oxford University Press; 1989:15–36.
10. Chang LT. A method for attenuation correction in radionuclide computed tomography. *IEEE Trans Nucl Sci* 1978;25:638–643.
11. Staff RT, Gemmell HG. A simple method for the correction of photon attenuation caused by patient couches in SPECT. *Phys Med Biol* 1991;36: 1693–1697.
12. Swets JA, Pickett RM. *Evaluation of diagnostic systems: methods from signal detection theory*. New York: Academic Press, 1982.
13. Metz CE, Wang P-L, Kronman HB. A new approach for testing the significance of differences between ROC curves measured from correlated data. In: Deconick F, ed. *Proceedings of information processing in medical imaging*. The Hague: Nijhoff, 1984:432–445.
14. Metz CE. ROC methodology in radiologic imaging. *Invest Radiol* 1986;21: 720–733.
15. Metz CE, Kronman HB. Statistical significance tests for binormal ROC curves. *J Math Psychol* 1980;22:218–243.
16. Dorfman DD, Alf E. Maximum likelihood estimation of parameters of signal detection theory and determination of confidence intervals—rating method data. *J Math Psychol* 1969;6:487–496.
17. Myers KJ, Barrett HH. Addition of a channel mechanism to the ideal observer model. *J Opt Soc Am A* 1987;4:2447–2457.